Effects of buffer layers on the structural and electronic properties of InSb films

X. Weng, N. G. Rudawski, P. T. Wang, and R. S. Goldman[a)]
Department of Materials Science and Engineering, University of Michigan, Ann Arbor, Michigan 48109-2136

D. L. Partin and J. Heremans
Delphi Research and Development Center, Warren, Michigan 48090-9055

(Received 7 July 2004; accepted 2 November 2004; published online 28 January 2005)

We have investigated the effects of various buffer layers on the structural and electronic properties of *n*-doped InSb films. We find a significant decrease in room-temperature electron mobility of InSb films grown on low-misfit GaSb buffers, and a significant increase in room-temperature electron mobility of InSb films grown on high-misfit InAlSb or step-graded GaSb+InAlSb buffers, in comparison with those grown directly on GaAs. Plan-view transmission electron microscopy (TEM) indicates a significant increase in threading dislocation density for InSb films grown on the low-misfit buffers, and a significant decrease in threading dislocation density for InSb films grown on high-misfit or step-graded buffers, in comparison with those grown directly on GaAs. Cross-sectional TEM reveals the role of the film/buffer interfaces in the nucleation (filtering) of threading dislocations for the low-misfit (high-misfit and step-graded) buffers. A quantitative analysis of electron mobility and carrier-concentration dependence on threading dislocation density suggests that electron scattering from the lattice dilation associated with threading dislocations has a stronger effect on electron mobility than electron scattering from the depletion potential surrounding the dislocations. Furthermore, while lattice dilation is the predominant mobility-limiting factor in these *n*-doped InSb films, ionized impurity scattering associated with dopants also plays a role in limiting the electron mobility. © *2005 American Institute of Physics*. [DOI: 10.1063/1.1841466]

I. INTRODUCTION

Due to its small direct band gap (0.17 eV), low effective mass (0.013 m_e), and high room-temperature electron mobility ($\sim 7\times 10^4$ cm^2/V s), InSb is useful for a variety of device applications, including infrared sources, detectors, and magnetoresistive sensors.[1] InSb films are generally grown on semi-insulating GaAs or InP substrates, with a 14.6% or 10.4% lattice mismatch, respectively. The high mismatch between the film and substrate often results in a high density of threading dislocations in the film. In general, the threading dislocation density decreases and the electron mobility increases as the InSb film thickness increases.[2] For example, we recently reported that electron scattering from the strain field associated with threading dislocations is the primary mobility-limiting mechanism in highly mismatched InSb films grown on GaAs.[2]

In principle, thin InSb films are often desired for device applications, such as magnetoresistive sensors, in order to facilitate a higher output voltage for a given bias current.[1] However, in thin InSb films grown directly on GaAs or InP substrates, the typically high density of threading dislocations significantly reduces the film electron mobility. Thus, interposition of a dislocation-filtering buffer layer between the film and substrate is needed. In addition, to minimize leakage current, the buffer needs to be highly resistive. Recently, highly mismatched resistive buffers such as InAlSb have shown promise for increasing the electron mobility of thin InSb films.[3–5] For example, the electron mobility of a 0.55-μm *n*-doped InSb film was increased to that of a 1.5-μm *n*-doped InSb/InP film by interposing a low Al composition InAlSb buffer layer between the film and InP substrate.[3] Similarly, the electron mobility of a 0.55-μm undoped InSb film was increased to that of a 1-μm undoped InSb/GaAs film by interposition of an $In_{0.88}Al_{0.12}Sb$ buffer.[4] In another study, the interposition of a 1-μm AlSb buffer and a 1-μm $In_xAl_{1-x}Sb$ step-graded buffer ($x=0.1-0.9$) led to a $\sim$20% increase in electron mobility for 2-μm InSb/GaAs films.[5]

The increases in electron mobilities for InSb/InP and InSb/GaAs with interposed InAlSb buffers were qualitatively attributed to a decrease in film threading dislocation densities. This assessment was based on optical microscopy examination of film surface defects, double-crystal x-ray diffraction measurements of InSb epilayer peak widths, and preliminary cross-sectional transmission electron microscopy (TEM) images, respectively.[3–5] However, a quantitative examination of the evolution of threading dislocations in InSb films grown on GaAs with interposed InAlSb buffers has not been reported. Thus, the effects of InAlSb buffer layers on the nucleation, propagation, and filtering of threading dislocations are not fully understood. Furthermore, a quantitative

[a)]Author to whom correspondence should be addressed; electronic mail: rsgold@engin.umich.edu

analysis of the effects of threading dislocations on electron mobilities of InSb films grown on InAlSb buffers has not been reported.

Another possible buffer for interposition between InSb and GaAs is GaSb. Since GaSb is highly resistive, with an intrinsic resistivity $\sim 10^5$ times of that of InSb at 300 K,[6] the leakage current through the GaSb buffer is expected to be insignificant. Furthermore, GaSb has a lattice parameter intermediate to GaAs and InSb. Thus, a GaSb buffer may be used to relax the misfit strain between the InSb film and the GaAs substrate, and to prevent strain relaxation-induced defects from propagating into the film. To date, GaSb has been used as the substrate for growth of InSb/GaSb quantum dots,[7–9] or the barrier layer of InSb/GaSb quantum wells.[10] However, the nucleation and evolution of dislocations in InSb/GaSb heterostructures have not been examined. Furthermore, the effects of a GaSb buffer on the evolution of threading dislocations and the InSb electron mobility in InSb/GaSb/GaAs heterostructures have not been reported.

Therefore, we have investigated the effects of InAlSb and/or GaSb buffers on the evolution of threading dislocations and electronic properties of *n*-doped InSb films. Plan-view TEM shows a significant decrease or increase in threading dislocation density for InSb films grown on InAlSb or GaSb layers, compared with those grown directly on GaAs. Cross-sectional TEM reveals bending or nucleation of threading dislocations at InSb/InAlSb or InSb/GaSb interfaces, suggesting that these interfaces play an important role in dislocation filtering and/or nucleation. The room-temperature electron mobility of *n*-doped InSb films grown on InAlSb or GaSb buffers increases or decreases significantly, in comparison with those grown directly on GaAs. We also show quantitatively that the lattice dilation scattering related to threading dislocations has a stronger effect on electron mobility than the depletion potential scattering associated with threading dislocations. In addition, ionized impurity scattering associated with dopants further reduces the electron mobility of these *n*-doped InSb films.

The article is organized as follows. In Sec. II, we describe the procedures used for the experimental studies, including molecular-beam epitaxial (MBE) growth, high-resolution x-ray diffraction (HRXRD), cross-sectional and plan-view TEM, and resistivity and Hall measurements. In Sec. III, the evolution of threading dislocations, including the role of various buffers in filtering or/and nucleation of threading dislocations, is presented. The relative effects of threading dislocations and impurities on film electron mobility are discussed in Sec. IV. Conclusions are given in Sec. V.

II. EXPERIMENTAL PROCEDURES

InSb films and InAlSb and GaSb buffer layers were grown on semi-insulating GaAs (001) substrates using a Veeco MOD Gen II MBE system, with solid In, Ga, Al, Be, and Sb_4 sources, as described elsewhere.[3,11,12] A PbTe source oven was used for Te *n*-type doping of the InSb films.[11] Prior to growth, all elemental fluxes were measured using a quartz-crystal deposition monitor at the growth position. During growth, the substrate temperatures were monitored

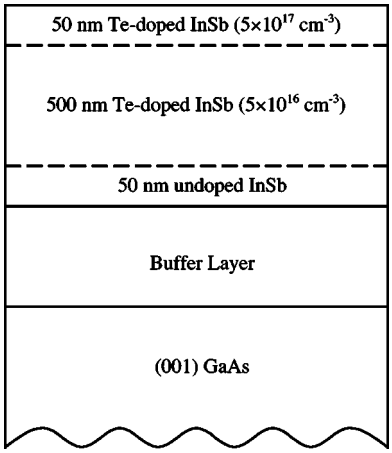

FIG. 1. Sample schematic for InSb films grown on low-misfit, high-misfit, and step-graded buffers.

using a Thermionics diffuse reflectance spectrometer (DRS)-1000. All the film and buffer nucleations were initiated at 330 °C, by alternately supplying metals and nonmetal (Sb), with a total of 90 periods, to a final thickness of ~ 30 nm.[13] Growth was then resumed in a conventional (continuous) growth mode at 410 °C.

Figure 1 shows a cross section of the targeted structures. Each structure consists of a 600-nm InSb film grown on a buffer layer. The buffer layers included 300-nm GaSb, 300-nm $In_{0.94}Al_{0.06}Sb$, or 27-nm GaSb plus 300-nm $In_{0.94}Al_{0.06}Sb$. Since GaSb and $In_{0.94}Al_{0.06}Sb$ have lattice mismatches of $\sim 7.8\%$ and $\sim 14.2\%$ with respect to the GaAs substrate, we will refer to the GaSb and InAlSb buffers as "low-misfit" and "high-misfit" buffers, respectively. In addition, we will refer to the GaSb+InAlSb buffer as the "step-graded" buffer. For undoped InAlSb, an earlier study showed an increase (decrease) in electron density (resistivity) with temperature.[3] On the other hand, Be-doped *p*-type InAlSb showed nearly constant resistivity over a significant temperature range. Therefore, in this study, the high-misfit buffer layers were doped with Be at $\sim 3\times 10^{17}$ cm^{-3} to maintain a high resistivity at high temperatures, which would minimize leakage current in potential magnetoresistive sensor applications.[3] Due to its high intrinsic resistivity ($\sim 10^5$ times of that of InSb), the low-misfit buffer was not intentionally doped. Each InSb film contains a Te-doping profile. At the bottom, a 50-nm undoped region separates the active region from the buffer. In the middle, a 500-nm region doped with $\sim 5\times 10^{16}$ cm^{-3} is the active region. At the top, a 50-nm region doped with $\sim 5\times 10^{17}$ cm^{-3} facilitates a low-resistance ohmic contact for potential magnetic-field sensing device applications.[3,14] For comparison, a "reference" sample, consisting of a 100-nm undoped InSb layer followed by a 500-nm InSb layer doped with Te at $\sim 1.2\times 10^{17}$ cm^{-3}, was also examined.

HRXRD measurements were performed using Cu $K\alpha$ radiation monochromated by a four-reflection Si(220) monochromator. For each sample, symmetric (004) and asymmetric (115) rocking curves and/or ω-2θ scans were collected at several azimuthal angles in order to take into account any nonzero angle of rotation of the epilayer planes about an

in-plane axis (epilayer tilt). In order to resolve the InSb and InAlSb peaks in samples with the high-misfit or step-graded buffers, a 140-μm slit was placed in front of the detector in the ω-2θ scans. Analysis of the HRXRD data reveals essentially complete relaxation of the InSb films, the high-misfit and low-misfit buffers, and the InAlSb layer of the step-graded buffer. For TEM studies, cross-sectional specimens were prepared using conventional mechanical thinning followed by argon-ion milling at 77 K. Plan-view TEM specimens were prepared using mechanical polishing followed by chemical etching from the substrate side. $NH_4OH/H_2O_2(4:1)$ and $HF/HNO_3/H_2O(1:1:4)$ were used to etch off the GaAs substrate and InSb films, respectively. TEM imaging and electron diffraction were carried out on a JEOL 2010FX transmission electron microscope operating at 200 keV. The plan-view TEM specimen thicknesses were determined using convergent beam electron diffraction.[15] The carrier concentrations and electron mobilities of the films were determined using room-temperature resistivity and Hall measurements, both in the van der Pauw configuration.[16]

III. EVOLUTION OF THREADING DISLOCATIONS

A. Overview

We quantified the threading dislocation densities in the InSb films using plan-view TEM. Figure 2 shows representative plan-view TEM images of InSb films grown on (a) GaAs, as well as on the (b) low-misfit, (c) high-misfit, and (d) step-graded buffers. We counted the number of threading dislocations over areas of ~73.6, 85.8, 139.1, and 78.9 μm^2 for films grown on GaAs, low-misfit, high-misfit, and step-graded buffers, respectively. The corresponding threading dislocation densities are $(1.4\pm0.2)\times10^9$ cm^{-2}, $(2.3\pm0.2)\times10^9$ cm^{-2}, $(5.9\pm0.8)\times10^8$ cm^{-2}, and $(6.1\pm0.8)\times10^8$ cm^{-2}, respectively. We note that the images of the InSb films grown on GaAs, or low-misfit or step-graded buffers, such as those in Figs. 2(a), 2(b), and 2(d) include only the top ~100 nm of the films. On the other hand, the images of the InSb films grown on high-misfit buffers, such as that in Fig. 2(c), include the top ~200 nm of the films. Thus, the apparent threading dislocation densities are artificially lower than the actual threading dislocation densities. However, as will be shown below, for all InSb films, the threading dislocation density decreases monotonically in the growth direction, similar to earlier studies of InSb films grown directly on GaAs.[2] Thus, for the high-misfit buffer, the threading dislocation density is lower for the top ~100 nm than for the top ~200 nm of the InSb film. It is therefore appropriate to conclude that the InSb film threading dislocation densities are lower for growth on high-misfit or step-graded buffers in comparison with low-misfit buffers and GaAs.

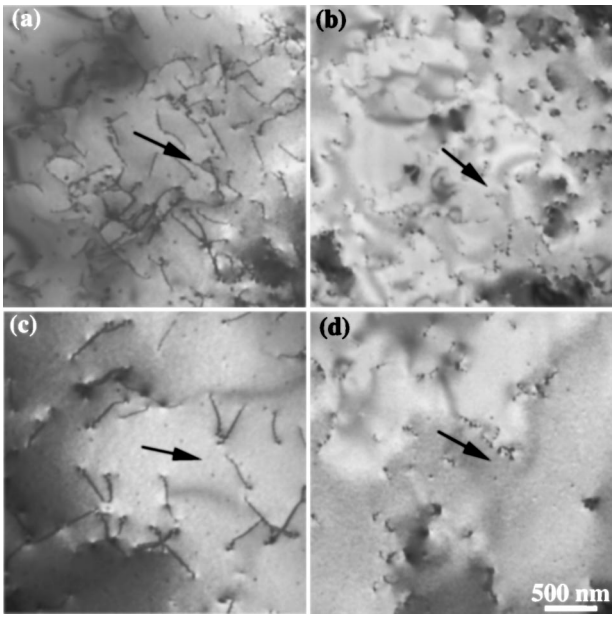

FIG. 2. Bright-field plan-view TEM images of InSb films grown on (a) GaAs, (b) low-misfit GaSb, (c) high-misfit InAlSb, and (d) step-graded GaSb+InAlSb buffers. All the images were collected near a two-beam condition with $\mathbf{g}=220$, which is in the direction of the black arrow in each image.

In order to understand the roles of low-misfit, high-misfit, and step-graded buffers in increasing or decreasing threading dislocation densities, we examined the evolution of threading dislocations within the films, buffer layers, and at the film/buffer/substrate interfaces using cross-sectional TEM. Figures 3(a), 3(c), 3(e), and 3(g) and Figs. 3(b), 3(d), 3(f), and 3(h) are representative low-magnification and high-magnification cross-sectional TEM images of InSb films grown on GaAs (the reference sample), the low-misfit, high-misfit, and step-graded buffers, respectively. In the following sections, we discuss the threading dislocation evolution in each buffer.

B. Reference sample

For InSb films grown directly on GaAs, the threading dislocation density decreases monotonically in the growth direction, similar to earlier studies of InSb films grown directly on GaAs.[2] A similar effect is observed for the InSb films grown on the buffers. For example, Fig. 3(b) shows a typical high-magnification cross-sectional TEM image of the reference sample. A high density of threading dislocations is apparent within ~20 nm of the InSb/GaAs interface. Beyond this region, the dislocation density decreases abruptly, due to several possible mechanisms, including the annihilation of dislocations with opposite Burgers vectors and the bending of dislocations to form half loops near the interface.[2,17]

C. Low-misfit buffer

Figure 3(d) shows the threading dislocation configurations near the low-misfit buffer. The threading dislocation density of the low-misfit buffer is apparently lower than that of the reference sample shown in Fig. 3(b) and discussed in Sec. III B above. Near the buffer/film interface, a high density of threading dislocations is apparent, suggesting the nucleation of threading dislocations at the buffer/film interface. As discussed earlier, the InSb film threading dislocation densities are higher for growth on the low-misfit buffer in comparison with GaAs substrates. This is likely due to dif-

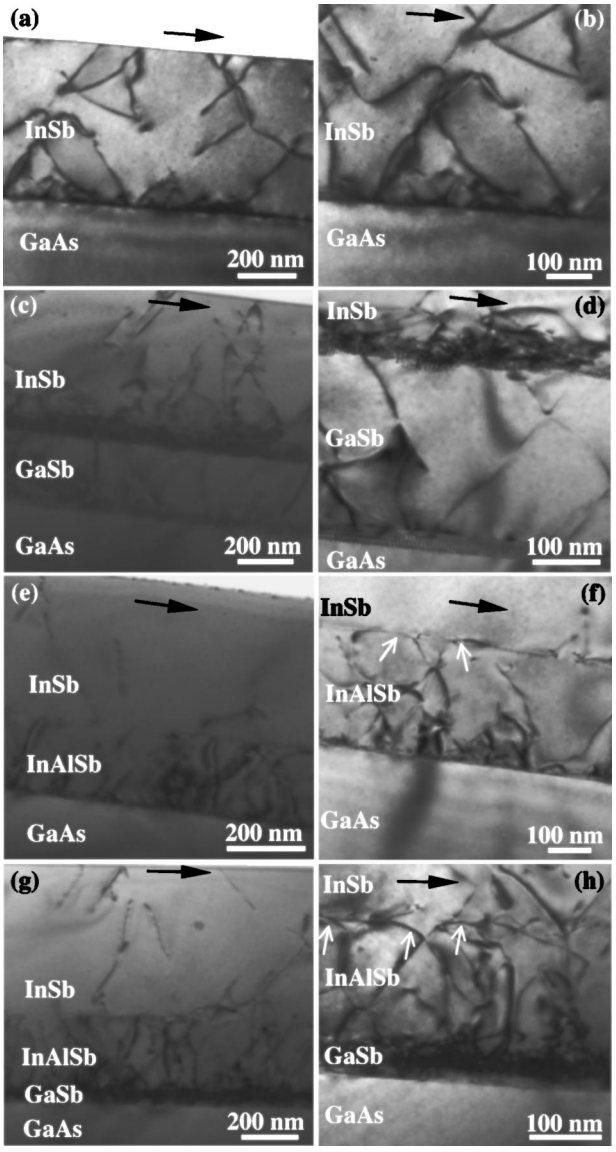

FIG. 3. Low-magnification bright-field cross-sectional TEM images of InSb films grown on (a) GaAs, (c) low-misfit GaSb, (e) high-misfit InAlSb, and (g) step-graded GaSb+InAlSb buffers. (b), (d), (f), and (h) are high-magnification images corresponding to (a), (c), (e), and (g), respectively. All the images were collected near a two-beam condition with $\mathbf{g}=220$, which is in the direction of the black arrow in each image. The white arrows in (f) and (h) indicate the bending of threading dislocations at the interfaces between the InSb films and buffers.

ferences in dislocation annihilation and bending at InSb/GaAs and InSb/GaSb interfaces, resulting from variations in growth modes and strain relaxation mechanisms.

In the InSb/GaAs system, InSb films initially grow in the Volmer–Weber mode, which consists of nucleation and coalescence of three-dimensional islands.[18] During the initial stages of growth, misfit dislocations may form in the InSb islands as grown-in dislocations. Alternatively, misfit dislocations may form at the InSb island edges as the islands grow and coalesce.[18] The cross-sectional TEM images shown in Refs. 2 and 18 indicate that threading dislocations often bend around the islands to form loops, which significantly reduce the percentage of threading dislocations entering the upper part of thick InSb films grown on GaAs.

On the other hand, on GaSb, InSb films typically grow in the Stranski–Krastanow mode, which consists of a two-dimensional layer-by-layer growth followed by elastic relaxation via three-dimensional island nucleation.[7] To date, a detailed investigation of the evolution of threading dislocations during the initial growth of InSb on GaSb is not available. In our case, during the initial stage of InSb growth on the low-misfit buffer, preexisting threading dislocations in the low-misfit buffer may thread through the wetting layer to form threading dislocations in the InSb layer. As the growth proceeds, misfit strain may be relaxed by the gliding of threading dislocations to form misfit segments at the InSb/GaSb interface. This strain relaxation via misfit dislocation formation may in turn suppress the island nucleation. Further relaxation of the misfit strain may also occur via the glide of dislocation half loops at the epilayer surface to the interface,[19,20] dislocation multiplication and interaction,[21–23] and dislocation nucleation at local stress concentrations due to contaminants, particulates, or stacking faults.[24,25]

D. High-misfit buffer

The high-misfit buffer contains a high density of threading dislocations within ~20 nm of the buffer/GaAs interface, and the threading dislocation density decreases monotonically in the growth direction, similar to the reference sample discussed earlier. At the buffer/film interface, several dislocations have bent, including two examples shown as white arrows in Fig. 3(f). During the InSb film growth, it is likely that preexisting threading dislocations glided at the interface, forming misfit dislocation segments, similar to earlier studies of compositionally graded buffers.[24,26–28] During the glide process, threading arms with opposite Burgers vectors may interact, leading to dislocation annihilation. In addition, some threading arms may glide to the edge of the sample.[24,26–28] These processes likely lead to the reduced threading dislocation density for InSb films growth on high-misfit buffers in comparison to GaAs substrates.

E. Step-graded buffer

Figure 3(h) shows the evolution of threading dislocations within the step-graded buffer, which consists of 27-nm GaSb plus 300-nm InAlSb layers. In the vicinity of the GaSb layer, significant strain contrast from a high density of dislocations dominates the image. The InAlSb layer threading dislocation densities are higher for growth on a thin GaSb layer (i.e., the step-graded buffer) in comparison with that directly on GaAs (i.e., the high-misfit buffer). This result suggests that the InAlSb/GaSb interface may act as a threading dislocation nucleation source, similar to the InSb/low-misfit buffer interface shown in Fig. 3(d). At the buffer/film interface, bending of threading dislocations is also evident, as indicated by the white arrows in Fig. 3(h). The bent threading dislocations likely contributed to both plastic relaxation and dislocation annihilation, similar to the high-misfit buffer case discussed in Sec. III D above.

TABLE I. The electron concentrations, n, electron mobilities, μ, and dislocation densities, D, of InSb films grown on GaAs and various buffer layers.

Buffer layer	n ($\times 10^{17}$ cm^{-3})	μ (cm^2/V s)	D (cm^{-2})
None (Ref. sample)	1.2	32 000	$(1.4\pm0.2)\times10^9$
Low-misfit	0.7	25 000	$(2.3\pm0.2)\times10^9$
High-misfit	0.7	43 000	$(5.9\pm0.8)\times10^8$
Step-graded	0.7	40 000	$(6.1\pm0.8)\times10^8$

IV. ELECTRONIC PROPERTIES

Table I presents the measured room-temperature electron concentrations, electron mobilities, and threading dislocation densities of n-doped InSb films grown on GaAs and various buffer layers. It is evident that the electron mobilities of InSb films grown on the low-misfit or high-misfit buffers are significantly lower or higher than those of the films grown directly on GaAs. Furthermore, the increase or decrease of the electron mobilities corresponds to a decrease or increase in threading dislocation densities, respectively. This strongly suggests that dislocation scattering plays an important role in limiting the electron mobilities of the n-doped InSb films, similar to the case of the undoped InSb grown directly on GaAs.[2] We note that the InSb film grown directly on GaAs has a doping and free-carrier concentration twice that of all other films; yet, its electron mobility is higher than the InSb film grown on the low-misfit buffer. This suggests that ionized impurity scattering associated with the dopants is not the predominant mobility-limiting factor in these n-doped InSb films.

According to Matthiessen's rule, the electron mobility of n-InSb, μ, may be related to μ_b and $\mu_\perp$ through

$$1/\mu = 1/\mu_b + 1/\mu_\perp, \tag{1}$$

where μ_b is the intrinsic electron mobility of the bulk material and $\mu_\perp$ is the mobility limited by dislocation scattering. Electrons may be scattered by the depletion potential surrounding the dislocations (Coulomb potential scattering) and the lattice dilation associated with the dislocation (deformation potential scattering).[29,30] The Pödör and Dexter–Seitz models consider free-carrier scattering from the depletion potential and the lattice dilation, respectively.[29,30] For highly mismatched undoped InSb films grown directly on GaAs, we found that the dominant factor limiting the room-temperature electron mobility was free-carrier scattering from the lattice dilation (Dexter–Seitz model).[2] Here, we consider the Pödör and Dexter–Seitz models to evaluate the effects of threading dislocations on the electron mobility of the n-doped InSb films grown on buffer layers.

According to the Pödör model,[29] the electron mobility limited by depletion potential scattering associated with dislocations, μ_C, is as follows:

$$\frac{1}{\mu_C} = \frac{e^2\sqrt{m^*}f^2}{30\sqrt{2\pi}(\varepsilon\varepsilon_0)^{3/2}\lambda^2 k_B T\sqrt{n}}\frac{D}{\sqrt{n}}, \tag{2}$$

where ε is the static dielectric constant, ε_0 is the permittivity of vacuum, $f \leqslant 1$ is the fraction of the filled traps along the dislocation lines, T is the absolute temperature, k_B is Boltzmann's constant, m^* and e are the electron effective mass and electron charge, λ is the unit crystallographic slip distance, and n is the electron concentration. Using a bulk mobility value of $\mu_b \approx 6\times10^4$ cm^{2}V s,[31] we plot $1/\mu$ as a function of $D/\sqrt{n}$, as predicted by the Pödör model in Fig. 4(a). We also include the experimentally determined values of $1/\mu$ as a function of $D/\sqrt{n}$ of the undoped InSb (Ref. 2) and n-doped InSb. Using a linear least-squares fit of the experimental data, we obtain a slope value of $\sim 2.54\times10^{-6}$ V s/cm$^{3/2}$ for the n-doped InSb, which is comparable to $\sim 2.86\times10^{-6}$ V s/cm$^{3/2}$ for the undoped InSb. Both slopes are approximately an order of magnitude larger than $\sim 2.90\times10^{-7}$ V s/cm$^{3/2}$, the maximum of the slope calculated from Eq. (3) using $f=1$, $\lambda = 3.9674$ Å and $\varepsilon = 17.8$.[2,32] These results suggest that the electron mobility and free-carrier concentration dependencies on threading dislocation density in both the n-doped and undoped InSb films are not primarily explained by the Pödör model.

On the other hand, according to the Dexter–Seitz model,[30] the mobility limited by deformation potential scattering associated with edge dislocations, μ_D, is inversely proportional to the edge dislocation density, D, as follows:

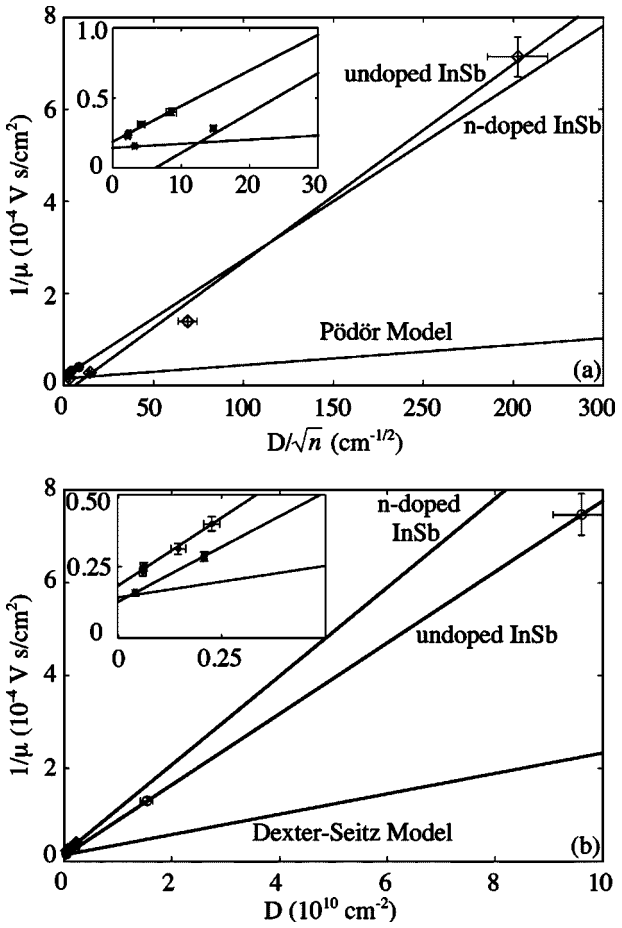

FIG. 4. Inverse electron mobility, $1/\mu$, as a function of (a) $D/\sqrt{n}$ and (b) D, where D and n are the dislocation density and carrier concentration, respectively. The experimental data for the n-doped and undoped InSb (Ref. 2), as well as the predictions by the Dexter–Seitz and Pödör models, are included. The insets show the initial portion of the plot of $1/\mu$ vs (a) $D/\sqrt{n}$ and (b) D.

$$\frac{1}{\mu_D}=\left[\frac{3\pi}{32}\left(\frac{1-2\nu}{1-\nu}\right)^2\frac{E_1^2\lambda^2 m^*}{k_B T\hbar e}\right]D, \tag{3}$$

where E_1 is the hydrostatic deformation potential,[33,34] and ν is the Poisson's ratio. Figure 4(b) shows the inverse of electron mobility, $1/\mu$, as a function of the threading dislocation density, D, for the *n*-doped InSb studied in this work. For comparison, the variation of $1/\mu$ with D for the undoped InSb films is also included.[2] In addition, we plot the predicted $1/\mu$ as a function of D using Eq. (1), with $\mu_\perp=\mu_D$, the dislocation scattering-limited mobility predicted by the Dexter–Seitz model. The slope of the predicted line, $\sim 2.20\times10^{-15}$ V s, is calculated using Eq. (2).[2] The bulk mobility value for *n*-InSb with a carrier concentration of $\sim 7\times10^{16}$ cm^{-3}, $\mu_b\approx 6\times10^4$ cm^2/V s, is used for the predicted line.[31] Using a linear least-squares fit of the experimental data, we obtain a slope value of $\sim 9.53\times10^{-15}$ V s for the *n*-doped InSb, which is comparable to $\sim 7.64\times10^{-15}$ V s for the undoped InSb, and $\sim 2.20\times10^{-15}$ V s, the value predicted by the Dexter–Seitz model.[2] The bulk mobility value obtained from the linear fitting of the experimental data is $\sim 5.49\times10^4$ cm^2/V s, slightly smaller than the reported value, $\sim 6\times10^4$ cm^2/V s.[31] These results show a quantitative correlation between increasing dislocation density and decreasing electron mobility, which is apparently consistent with the predictions of the Dexter–Seitz model.

We note that the dislocation densities may be underestimated by up to a factor of 2, due to the fact that we have imaged only the top $\sim 1/6-1/3$ of the InSb films. Such variations produce up to a factor of 2 variation in the slope values for both the Pödör and Dexter–Seitz models, without a consequent variation in the bulk mobility. Hence, the possible underestimation of the dislocation densities does not alter the assertion that the Dexter–Seitz model is more suitable for describing the variation of electron mobility and concentration with the threading dislocation density. Taken together, these results suggest that lattice dilation scattering has a stronger effect than the depletion potential scattering on the electron mobility in the *n*-doped InSb films.

The insets of Fig. 4 show the initial portion of the plot of $1/\mu$ vs (a) $D/\sqrt{n}$ and (b) D. For the *n*-doped InSb films, the linear least-squares fit to $1/\mu$ vs $D/\sqrt{n}$ or D lies above that of the undoped InSb films and those predicted by the Pödör model or the Dexter–Seitz model, indicating lower mobility values in this case. These results suggest that dislocation scattering is the predominant mobility limiting mechanism in *n*-doped InSb films, while electron scattering associated with ionized impurities also plays a role.

V. CONCLUSIONS

In summary, we have investigated the effects of various buffer layers on the structural and electronic properties of *n*-doped InSb films grown on low-misfit GaSb, high-misfit InAlSb, and step-graded GaSb+InAlSb buffer layers. At the InSb/low-misfit buffer interface, threading dislocations nucleate, significantly increasing the dislocation density in the InSb films. On the other hand, at the InSb/high-misfit and InSb/step-graded buffer interfaces, threading dislocations bend, thus significantly decreasing the dislocation density in the InSb films. The electron mobility decreases (increases) significantly for InSb films grown on low-misfit (high-misfit or step-graded) buffers, in comparison to GaAs substrates, apparently due to the increase (decrease) in threading dislocation densities. A quantitative analysis of the correlation between the dislocation density and the electron mobility and carrier concentration suggests that the lattice dilation scattering has a stronger effect on the electron mobility than the depletion potential scattering related to threading dislocations. Both dislocation scattering and ionized impurity scattering associated with dopants play important roles in limiting the electron mobility.

ACKNOWLEDGMENTS

This work was supported in part by the National Science Foundation (NSF) under Grant Nos. 9773707 and 0210714. The authors also acknowledge the assistance of the staff of Electron Microbeam Analysis Laboratories (EMAL) at the University of Michigan. The JEOL 2010 FX analytical electron microscope at EMAL is supported by NSF under Grant No. 9871177.

[1] J. Heremans, J. Phys. D **26**, 1149 (1993).
[2] X. Weng, R. S. Goldman, D. L. Partin, and J. P. Heremans, J. Appl. Phys. **88**, 6276 (2000).
[3] D. L. Partin, J. Heremans, and C. M. Thrush, J. Vac. Sci. Technol. B **17**, 1267 (1999).
[4] R. M. Biefeld and J. D. Phillips, J. Cryst. Growth **209**, 567 (2000).
[5] T. Sato, M. Akabori, and S. Yamada, Physica E (Amsterdam) **21**, 615 (2004).
[6] M. Levinshtein, S. Rumyantsev, and M. Shur, *Handbook Series on Semiconductor Parameters*, Vol. 1 (World Scientific, Singapore, 1996).
[7] N. Bertru, O. Brandt, M. Wassermeier, and K. Ploog, Appl. Phys. Lett. **68**, 31 (1996).
[8] P. Möck, G. R. Booker, N. J. Mason, R. J. Nicholas, E. Aphandéry, T. Topuria, and N. D. Browning, Mater. Sci. Eng., B **80**, 112 (2001).
[9] A. F. Tsatsul'nikov *et al.*, Semiconductors **33**, 886 (1999).
[10] L. Q. Qian and B. W. Wessels, Appl. Phys. Lett. **63**, 628 (1993).
[11] D. L. Partin, J. Heremans, and C. M. Thrush, J. Appl. Phys. **71**, 2328 (1992).
[12] D. L. Partin, J. Heremans, and C. M. Thrush, J. Cryst. Growth **175/176**, 860 (1997).
[13] G. S. Lee, P. E. Thompson, J. L. Davis, J. P. Omaggio, and W. A. Schmidt, Solid-State Electron. **36**, 387 (1993).
[14] D. L. Partin, J. Heremans, and C. M. Thrush, Sens. Actuators, A **69**, 39 (1998).
[15] D. B. Williams and C. Barry Carter, *Transmission Electron Microscopy* (Plenum, New York, 1996), p. 321.
[16] L. J. van der Pauw, Philips Res. Rep. **13**, 1 (1958).
[17] S. D. Parker *et al.*, Semicond. Sci. Technol. **4**, 663 (1989).
[18] X. Zhang, A. E. Staton-Bevan, D. W. Pashley, S. D. Parker, R. Droopad, R. L. Williams, and R. C. Newman, J. Appl. Phys. **67**, 800 (1990).
[19] D. Cherns and M. J. Stowell, Scr. Metall. **7**, 489 (1973).
[20] K. Yagi, K. Takayanagi, K. Kobayashi, and G. Honjo, J. Cryst. Growth **9**, 84 (1971).
[21] F. K. LeGoues, B. S. Meyerson, and J. F. Morar, Phys. Rev. Lett. **66**, 2903 (1991).
[22] A. Lefebvre, C. Herbeaux, C. Bouillet, and J. Di Persio, Philos. Mag. Lett. **63**, 23 (1991).
[23] J. Washburn and E. P. Kvam, Appl. Phys. Lett. **57**, 1637 (1991).
[24] R. Hull and J. C. Bean, Crit. Rev. Solid State Mater. Sci. **17**, 507 (1992).
[25] Y. Chen, Z. Liliental-Weber, J. Washburn, J. F. Klem, and J. Y. Tsao, Appl. Phys. Lett. **66**, 499 (1995).
[26] P. M. Mooney, Mater. Sci. Eng., R. **17**, 105 (1996).
[27] E. A. Fitzgerald, Mater. Sci. Rep. **7**, 87 (1991).
[28] F. K. LeGoues, Phys. Rev. Lett. **72**, 876 (1994).
[29] B. Pödör, Phys. Status Solidi **16**, K167 (1966).

[30]D. L. Dexter and F. Seitz, Phys. Rev. **86**, 964 (1952).
[31]E. Litwin-Staszewska, W. Szymanska, and R. Piotzkowski, Phys. Status Solidi B **106**, 551 (1981).
[32]M. Neuberger, *Handbook of Electronic Materials*, Vol. 2 (IFI/Plenum, New York, 1971), p. 79.
[33]J. Bardeen and W. Shockley, Phys. Rev. **80**, 72 (1950).
[34]C. G. Van de Walle, Phys. Rev. B **39**, 1871 (1989).